0022-3565/11/3392-421–429$25.00
THE JOURNAL OF PHARMACOLOGY AND EXPERIMENTAL THERAPEUTICS
Copyright © 2011 by The American Society for Pharmacology and Experimental Therapeutics
JPET 339:421–429, 2011

Vol. 339, No. 2
185249/3724326
Printed in U.S.A.

Multimodal Biomarker Investigation on Efficacy and Mechanism of Action for the Mammalian Target of Rapamycin Inhibitor, Temsirolimus, in a Preclinical Mammary Carcinoma OncoMouse Model: A Translational Medicine Study in Support for Early Clinical Development

Xinkang Wang, Yutian Zhan, Lei Zhao, John Alvarez, Inder Chaudhary, Bin-Bing Zhou, Robert T. Abraham, and Giora Z. Feuerstein

Imaging Biomarker Laboratory, Translational Medicine, Pfizer, Collegeville, Pennsylvania (X.W., Y.Z., L.Z., J.A., G.Z.F.); and Oncology and Hematology (I.C.) and Discovery Oncology (B.-B.Z., R.T.A.), Pfizer, Pearl River, New York

Received June 23, 2011; accepted August 10, 2011

ABSTRACT

The mammalian target of rapamycin (mTOR) has proven to be a valid therapeutic target in a number of human cancers, and it is a candidate for clinical trials in human breast cancer. We report on a biomarker-based translational medicine approach to assess the efficacy and mechanism of action for the mTOR inhibitor temsirolimus (CCI-779) in a mammary carcinoma OncoMouse model [polyomavirus middle T antigen (PyMT)]. The mTOR signaling pathway biomarkers were assessed using a reverse-phase protein array. Pharmacokinetics studies were conducted in both the tumor and plasma compartments. Pharmacodynamic biomarkers for compound-target engagement of tumor phospho-S6 proteins were assayed by Western blot. Temsirolimus (intravenously once a week for 2 weeks) was administered in both early and advanced stages of tumors. Biomarkers for temsirolimus effects on tumor progression were assessed by three-dimensional ultrasound imaging in combination with immunohistochemistry to assess vascular density (Texas red-dextran and CD31 immunostaining) and macrophage burden (F4/80 antigen). Tumor growth was significantly arrested in temsirolimus (25 $\pm$ 14% from 8 to 10 weeks, $p < 0.05$, and 26 $\pm$ 17% from 11 to 13 weeks, $p < 0.01$), compared with 493 $\pm$ 160 and 376 $\pm$ 50% increases, respectively, in vehicle-treated groups. Temsirolimus reduced tumor vascular density, 36 to 48 and 58 to 60%, $p < 0.05$, by the Texas red-dextran method or CD31-positive vessel count, respectively. Temsirolimus reduced tumor macrophage burden by 46% at 13 weeks ($p < 0.05$). Temsirolimus inhibited ($p < 0.05$) the phosphoproteins S6 pS235/236 and S6 pS240/244 up to 81 and 87%, respectively. We conclude that the multimodal biomarkers of temsirolimus efficacy and mechanism of action (phosphoproteins) strongly suggest that it might translate to therapeutic efficacy in human tumors that bear congruency to features present in the mammary carcinoma of PyMT tumors.

Introduction

The mammalian target of rapamycin (mTOR) is a valid therapeutic target in cancers (Abraham and Eng, 2008). mTOR is a downstream mediator in the phosphatidylinositol-3 kinase (PI3K)/Akt (protein kinase B) signaling pathway, which receives input from multiple signals (including growth factors and nutrients) to regulate protein synthesis through two main pathways, ribosomal S6 kinase (S6K) 1 and 2, and eukaryotic initiation factor 4E-binding protein 1, that play fundamental roles in ribosome biogenesis and cap-dependent translation, respectively (Brown et al., 1995; Brown and Schreiber, 1996). Rapamycin, a bacterially derived natural product, has been shown to be an immunosuppressant and anticancer agent (Sehgal et al., 1994; Huang et al., 2003). Both immunosuppressive and anticancer properties of rapamycin are attributed, at least in part, to its mTOR signaling pathway inhibition by controlling mRNA translation and cell proliferation. CCI-779 (temsirolimus), a synthetic analog of rapamycin, is an inhibitor of mTOR that is marketed for treatment of human renal carcinoma and has

Article, publication date, and citation information can be found at http://jpet.aspetjournals.org.
doi:10.1124/jpet.111.185249.

ABBREVIATIONS: mTOR, mammalian target of rapamycin; PyMT, polyomavirus middle T antigen; PI3K, phosphatidylinositol-3 kinase; S6K, ribosomal S6 kinase; MMTV, mouse mammary tumor virus; IHC, immunohistochemistry; PK, pharmacokinetic; VEGF, vascular endothelial growth factor; DAPI, 4,6-diamidino-2-phenylindole.

shown activity against a wide range of cancers in preclinical models (Geoerger et al., 2001; Neshat et al., 2001; Podsypanina et al., 2001; Yu et al., 2001; Frost et al., 2004; Teachey et al., 2006; Fung et al., 2009), including those of breast cancer xenografts (Yu et al., 2001; Fung et al., 2009). It is noteworthy that although temsirolimus demonstrated positive outcome in breast cancer xenografts, it was more effective for the therapeutics in human prostate cancer xenografts (Fung et al., 2009).

Mammary gland-specific expression of polyomavirus middle T antigen (PyMT) under the control of the mouse mammary tumor virus (MMTV) promoter in transgenic mice (MMTV-PyMT; cited as PyMT mice here) results in the transformation of mammary gland epithelium, leading to the development of multifocal mammary adenocarcinomas and metastasis to lymph nodes and the lung (Guy et al., 1992; Lin et al., 2003). Tumor formation and progression in these mice is characterized by four stages: hyperplasia, adenoma/mammary intraepithelial neoplasia, and early and late carcinoma (Lin et al., 2003). The congruency of this model to some forms of human breast cancer is exemplified by its gradual loss of steroid hormone receptors (estrogen and progesterone) and β1-integrin that is associated with overexpression of ErbB2 (HER2) and cyclin D1 in late-stage metastatic cancer (Maglione et al., 2001; Lin et al., 2003). The PyMT mouse model of breast cancer is further typified by short latency, high penetrance, and a high incidence of lung metastasis in the late stage (Lin et al., 2003). Furthermore, the immune-competent feature of PyMT mice provides advantages for tumor-associated inflammation relative to tumor xenografts. Taken together, these studies suggest that PyMT mice could serve as a useful preclinical model for evaluating the efficacy and mechanism of action of agents against tumor survival pathways such as the mTOR.

Because the role of the mTOR signaling pathway in PyMT-induced mammary tumorigenesis remains unclear, we embarked on an investigation of the mTOR pathway in this model using a multimodal biomarkers approach. We aimed to validate this model by using biomarkers for mTOR signaling pathway activation and probe the efficacy of CCI-779 to modify tumor growth kinetics along with several key tumor microenvironment and growth-promoting elements, including vasculogenesis and inflammation, that might govern tumor progression. The studies were conducted after pilot experiments that defined an optimal drug exposure along with pharmacokinetic and pharmacodynamic assessment. Tumor progression and regression were monitored using noninvasive ultrasound imaging. Tumor vasculogenesis and macrophages were evaluated by quantitative immunohistochemistry (IHC). These biomarker-based studies provide new insights into the mechanism of action and efficacy of rapamycin-related drugs toward PyMT-driven mammary tumors.

Materials and Methods

PyMT Mice. FVB/N-Tg (MMTV-PyMT)634Mul/J (PyMT) transgenic mice were provided by The Jackson Laboratory (Bar Harbor, ME). Heterozygous female PyMT mice were used for the present study. Genotype was determined by polymerase chain reaction using primers 5′-CAAATGTTGCTTGTCTGGTG-3′ and 5′-GTCAGTCGAGTGCACAGTTT-3′ as forward and reverse primers, respectively, for wild-type gene (200 base pairs) and 5′-GGAAGCAAGTACTTCACAAGGG-3′ and 5′-GGAAAGTCACTAGGAGCAGGG-3′ for PyMT transgenic gene (556 base pairs). Mice were housed and cared for in accordance with the *Guide for the Care and Use of Laboratory Animals* (Institute of Laboratory Animal Resources, 1996). The Institutional Animal Care and Use Committees approved all procedures described in this study.

Study Design. After pilot study on tumor progression in PyMT mice, using validated ultrasound technology (Zhao et al., 2010), both early (8–10 weeks of age) and advanced (11–13 weeks) tumors in mice were selected for the present study. Pharmacokinetic (PK) studies of CCI-779 and its metabolite rapamycin were conducted in PyMT mice after a single dose of 25 mg/kg i.v. CCI-779. Pharmacodymanic biomarkers, phospho-S6 cluster proteins, were measured by Western blot analysis. Ultrasound was used for noninvasive monitoring of tumor growth (volume) before and after two treatments (once a week) of CCI-779. This study was guided by pilot, dose-dependent (vehicle, 5 and 25 mg/kg i.v. CCI-779, once weekly) and time-dependent (treatment for 1–4 weeks) pharmacological studies in PyMT mice. The doses of CCI-779 at 5 and 25 mg/kg were selected according to previous studies in xenograft models (Yu et al., 2001 and Frost et al., 2004), of which 5 mg/kg was expected to have the least and 25 mg/kg the maximum efficacy without adverse effects. Tumor vascular density was evaluated by two methods: IHC using a fluorescence agent, Texas red-dextran, and an endothelium marker, CD31. Tumor macrophage burden was evaluated by IHC using an F4/80 antibody (for a pan-specific macrophage marker) as described previously (Lin et al., 2003).

Assessment of Tumor Volume by Ultrasound Imaging. In each mouse, the largest (single) tumor was measured by ultrasound (Vevo 770 high-resolution in vivo micro-imaging system; VisualSonics Inc., Toronto, Canada) according to the manufacturer's specification. Tumor volume was acquired through three-dimensional reconstruction of two-dimensional tumor panels uniformly spaced at defined intervals using the software provided by the manufacturer (Vevo 770 Analytic Software; VisualSonics, Inc.) (Zhao et al., 2010). The correlation between three-dimensional volume and the total tumor burden (by weight at postmortem) was validated in the same mouse.

In Vivo Vessel Labeling and Histological Analysis. Texas red-conjugated dextran (molecular weight 70,000; Molecular Probes, Carlsbad, CA) was used for in vivo labeling of tumor vasculature as described previously (Lin et al., 2006), using 6.2 mg/ml in phosphate-buffered saline; 21 μg/g of mouse body weight, intravenously injected 5 min before euthanasia. Tumors were isolated and preserved by either freezing or being formalin-fixed and paraffin-embedded, then sectioned for histological assessment of vascular density. For quantitative analysis of vessel distribution in the tumor, the images of the entire midline section of the largest tumor were captured with a Zeiss Axio Imager equipped with an automatic motorized stage (Carl Zeiss, Inc., Thornwood, NY). Texas red-dextran signals were analyzed using the Axio Imager data analysis program (Carl Zeiss, Inc.). The numbers of animals used for the studies are indicated in each figure legend.

Immunohistochemical Analysis. Rat monoclonal (CI:A3–1) anti-F4/80 antibody against a pan macrophage marker, BM8 (Abcam Inc., Cambridge, MA) was used to detect tumor macrophages as described previously (Lin et al., 2006), and rat anti-mouse CD31 antibody (BD Biosciences, San Jose, CA) was used to assess the total tumor vasculature. Standard procedure was used for the IHC analysis except that frozen sections were required for CD31 immunostaining using tissues fixed in 5% formalin in 20% sucrose/phosphate-buffered saline solution at 4°C for 24 h. Because of tumor heterogeneity, the photomicrographs of the immunoreactive signals from the entire tumor area were captured using the Zeiss Axio Imager equipped with an automatic motorized stage, and the areas were quantified (as the percentage of the total tumor area) by using the Axio Imager data analysis program. At least three sections from each animal ($n = 6$) were used to study the effects of CCI-779.

Drug Dosing and PK Analysis. CCI-779 (Pfizer, Collegeville, PA) was dissolved in a vehicle containing 2% Tween 80, 4% ethanol, and 5% polyethylene glycol 400 in water (as a stock solution for compound preparation) and mixed with 5% dextrose containing 0.25% lactic acid. Vehicle or 5 or 25 mg/kg CCI-779 was dosed intravenously via the tail vein once a week for 2 weeks.

PK study ($n = 3$) was performed in 11-week-old PyMT mice after a single dose of 25 mg/kg i.v. CCI-779. In our initial PK study, both plasma and tumor samples were collected at time 0, 1, 3, and 7 days after a single dosing. PK study at early time points was also conducted for both plasma and tumor drug concentrations for CCI-779 and its metabolite, rapamycin, at 0, 5, 15, and 30 min and 1, 6, 24 h after a single dose of 25 mg/kg i.v. Drug concentrations in plasma and tumor were determined by liquid chromatography/tandem mass spectrometry. Tumors were homogenized in 1:10 volume of water. The limitation of quantification for mass spectrometry is 1 ng/ml drug using a 50 μl of plasma and/or tumor. The specific extraction and reconstitution procedure included: 1) 50 μl of plasma sample or plasma for standard was loaded in each well of a 96-deep wall plate; 2) 50 μl of water was added to each sample and standard; 3) 10 μl of internal standard (either CCI-779 or rapamycin) was added (for a standard curve at 1–2500 ng/ml) and votexed for 5 min; 4) 400 μl of acetonitrile was added and votexed for 5 min; 5) for separation, samples were centrifuged at 3400 rpm for 10 min at 4°C; 6) 350 μl of supernatant was transferred into a 3M Empore filter plate (3M, St. Paul, MN) using the Tomtec Quadra 96 (Tomtec, Hamden, CA) and dried under nitrogen at 30°C; 7) samples were reconstituted with 200 μl of water/methanol (1:1); and 8) 10 μl of the reconstituted solution was injected into a liquid chromatographer/mass spectrometer for analysis. Chromatographic separation was performed using an Agilent 1200 LC system (Agilent Technologies, Santa Clara, CA), which was equipped with an ESI FlouroSep-RP phenyl HS 50 × 2.1 mm, 5-μ column. The mobile phase consisted of 10 mM ammonium acetate in water (solvent A) and 10 mM ammonium acetate in acetonitrile (solvent B). A gradient with a flow rate of 0.5 ml/min was initiated at 95% solvent A, increased to 95% solvent B at 4.5 min, and changed back to 95% solvent A for another 1.5 min. The mass spectrometry (using Sciex API-4000-Einstein Model ESI+; Applied Biosystems, Foster City, CA) conditions include multiple reaction monitoring, turbo ion-spray voltages at 5000 kV, and temperature at 500°C.

Western Blot Analysis. Antibodies targeting total S6 and phospho-S6, pS235/236, and pS240/244 proteins and anti-β-actin were purchased from Cell Signaling Technology (Danvers, MA). Tumor samples were collected from PyMT mice treated with CCI-779 or vehicle ($n = 3$) and immediately frozen in liquid nitrogen. Western blots were conducted on pulverized tumors after porcelain mortar and pestle grinding under liquid nitrogen. Western blotting was used to detect the phosphoproteins and nonphosphoproteins, and the specific band intensity was quantified as described previously (Wang et al., 2003).

mTOR Pathway Analysis. To validate the activation of mTOR signaling pathway in PyMT mice, the proteins and phosphoproteins, Akt, Akt pS473, Akt pT308, mTOR pS2488, p70S6K, P70S6K pT389, S6, S6 pS235/236, and S6 pS240/244 were analyzed in tumors isolated from 13-week-old mice ($n = 5$). Tumors were rapidly dissected out and immediately frozen in liquid nitrogen. The pulverized tissues were used for reverse protein array analysis by Bay Point Biosystems Inc. (Houston, TX) as described previously (Grote et al., 2008).

Statistical Analysis. All data are presented as mean ± S.E. Statistical comparisons were made by analysis of variance (with mean differences determined using Fisher's protected least-squares difference) test. Values were considered to be significant when $p < 0.05$ for CCI-779-treated groups compared with vehicle-treated groups as indicated in figure legends.

Results

mTOR Signaling Pathway Analysis. Figure 1 illustrates the PI3K/Akt/mTOR signaling pathway (Abraham and Eng, 2008; Le Tourneau et al., 2008) and the histogram data of the selected proteins and phosphoproteins of the mTOR signaling pathway detected by a reverse-phase protein array in the tumors of 13-week old PyMT mice ($n = 5$). The following proteins/phosphoproteins were evaluated in this study:

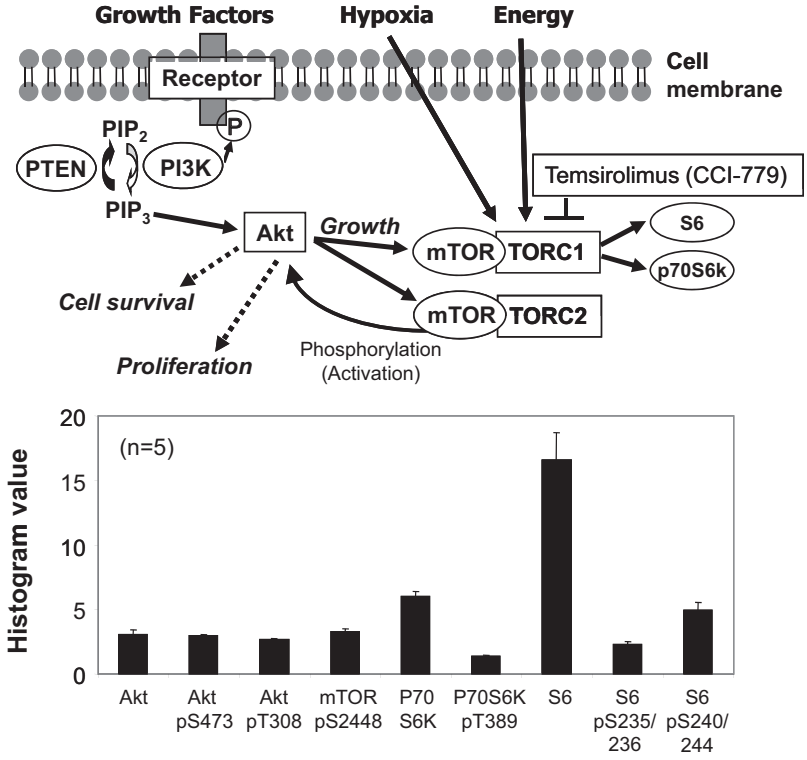

Fig. 1. Illustration of the mTOR signaling pathway (top) and expression of selected members of this pathway in PyMT mouse tumors (bottom). Tumors from PyMT mice at 13 weeks of age ($n = 5$) were dissected and used to study the mTOR signaling pathway by means of a reverse-phase protein array. The relative signal intensity in each protein/phosphoprotein was normalized against the standard and illustrated (bottom) as histograms in linear values converted from the raw data in $\log^2$ values ($n = 5$).

Akt, Akt pS473, Akt pT308, mTOR pS2448, P70S6K, P70S6K pT389, S6, S6 pS235/236 and S6 pS240/244. Although various levels of expression were observed, every member evaluated within this pathway was detected within the acceptable sensitivity of the methodology applied for the PyMT tumors. The maximum inhibition of S6 pS235/236 and S6 pS240/244 phosphoproteins reached 81 and 87%, respectively, at 1 to 6 h in the tumors after CCI-779 dosing (Fig. 1).

Pharmacokinetics of CCI-779 in PyMT Mice. PK study was conducted for both CCI-779 and its metabolite, rapamycin, in both plasma and tumors after a single dose of 25 mg/kg i.v. in PyMT mice. Plasma rapamycin levels reached peak immediately after dosing (27,500 ng/ml or 30,085 nM at 5 min) and remained elevated throughout 24 h (690 ng/ml or 755 nM at 24 h; Fig. 2A, top), whereas plasma CCI-779 levels reached peak (10,556 ng/ml or 11,548 nM at 5 min) and significantly diminished (1.7 ng/ml or 2 nM at 24 h). In contrast, concentrations for both compounds in tumors remained substantially higher (47 ng/ml or 51 nM for CCI-779 and 123 ng/ml or 135 nM for rapamycin in the tumors 24 h after dosing; Fig. 2A, top) and could still be detected 7 days after dosing (Fig. 2A, bottom; no data were available for rapamycin up to 7 days). As the result, the ratio of tumor/plasma drug was significantly higher for CCI-779 than rapamycin. Our additional studies showed a similar level of drug exposure in tumors for CCI-779 and rapamycin at 7 days after treatment of CCI-779, 25 mg/kg/week i.v. for 2 weeks (data not shown). A rapid decrease of CCI-779 in plasma in first 24 h (Fig. 1, top) may reflect the biodistribution of this compound and its quick conversion to metabolites (as shown for the sustained plasma levels of rapamycin), whereas a sustained level for a longer time (up to 7 days; Fig. 1, bottom) may reflect the long half-life of the compound and/or continued release from previously retained compartment such as tumors.

Effect of CCI-779 on S6 and Phospho-S6 Protein Expression by Western Blot. As illustrated in Fig. 3, total S6 protein levels were maintained at a similar level up to 24 h after CCI-779 administration, yet both phospho-S6 S235/236 and S6 S240/244 proteins rapidly declined (starting at 15 min) and reached statistically significance at 60 min after dosing (Fig. 3).

CCI-779 Effect on Tumor Growth. Significant inhibition of tumor growth progression was observed for both 5 and 25 mg/kg treatment regimens after 1 week and was sustained through the entire course of the study (Fig. 4A). The correlation between the ultrasound assessment and direct tumor weight was determined in 27 animals collected from three experiments. Correlation was established, with coefficient of $r^2 = 0.80$ (Fig. 4B). It was also noted that significant correlation was also established in the subgroup with total tumor burden <2 g ($r^2 = 0.88$, $n = 18$ for tumor weight <2 g).

Effects of CCI-779 on Imaging Biomarkers for Tumor Growth in Early and Advanced Tumors. As shown in Fig. 5, CCI-779, 25 mg/kg/week i.v. for 2 weeks, significantly reduced tumor volume ($n = 6$), with 25 ± 14% increases in animals from weeks 8 to 10 ($p < 0.05$) and 26 ± 17% decreases from weeks 11 to 13 ($p < 0.01$) compared with 493 ± 160 and 376 ± 50% increases, respectively, in vehicle-treated groups (Fig. 5).

Effects of CCI-779 on Biomarkers for Tumor Microvasculature in Early and Advanced Tumors. As shown in Fig. 6, mice ($n = 6$) treated with CCI-779, 25 mg/kg/week i.v. for 2 weeks, significantly reduced tumor vascular density, with 36 ± 6 and 58 ± 9% decreases ($p < 0.05$) at 10 and 13 weeks, respectively, based on Texas red-dextran perfusion

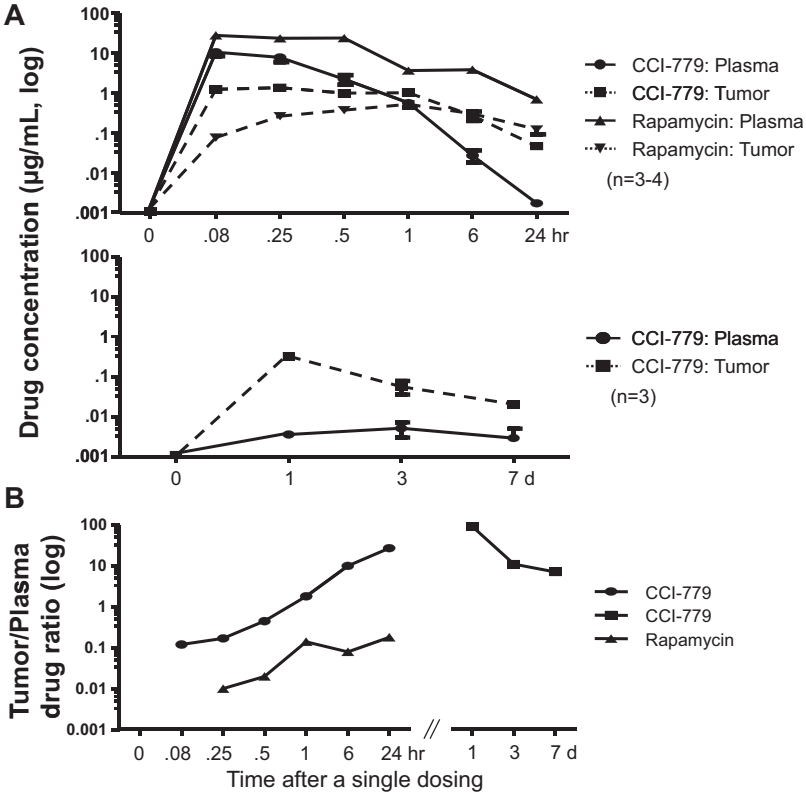

Fig. 2. Tumor and plasma pharmacokinetics for CCI-779 and its metabolite rapamycin in PyMT mice. A, mice were subjected to a single dose of 25 mg/kg CCI-779 through tail vein administration. Both plasma and tumor samples were collected at various time points as indicated and processed for CCI-779 and/or rapamycin drug concentration measurement as described in detail under *Materials and Methods*. B, the ratio of tumor/plasma drug exposure is illustrated according to the data shown in A. Rapamycin concentration was not measured for the 1- to 7-day study.

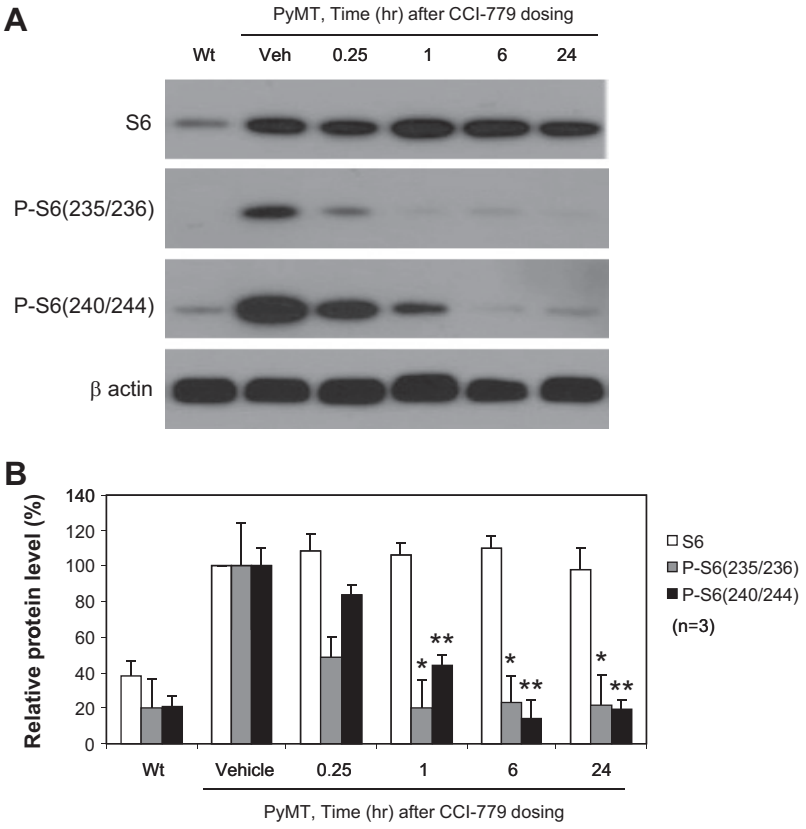

Fig. 3. Effects of CCI-779 on S6 and phosphor-S6 protein expression in PyMT breast tumors. The same animals (n = 3) subjected to a single dose of 25 mg/kg CCI-779 (as illustrated in Fig. 2 at various time points) were used for Western blot analysis as described in detail under *Materials and Methods*. A, representative Western blotting assays. Normal breast tissue from wild-type littermates (Wt) was used as control. B, quantitative data (n = 3) are illustrated in reference to vehicle samples as 100% for each protein (S6, pS6 S235/236, or pS6 S240/244) after normalizing the loading difference on the gel against the housekeeping gene β-actin.

areas in CCI-779 treated animals over vehicles or 48 ± 5 and 60 ± 17% decreases ($p < 0.01$) at 10 and 13 weeks, respectively, based on CD31-positive immunostaining vascular area.

Effects of CCI-779 on Biomarkers for Macrophage Infiltration in Early and Advanced Tumors. Representative immunohistochemical images in mice at 10 and 13 weeks after vehicle or 25 mg/kg/week CCI-779 (intravenously

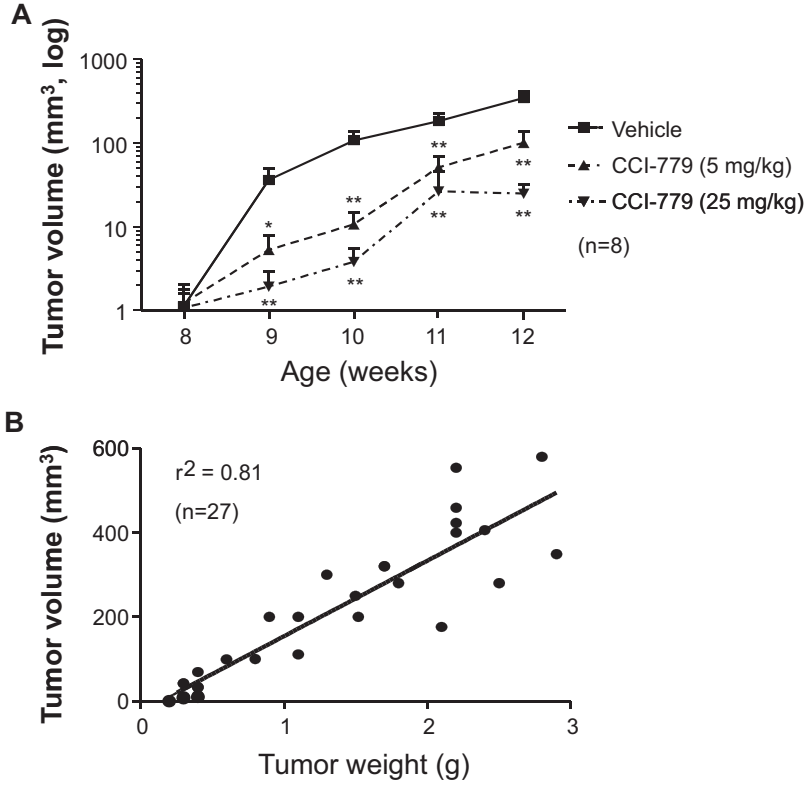

Fig. 4. Dose-dependent effect of CCI-779 on tumor progression in PyMT mice by means of ultrasound analysis. A, dose-dependent effect of CCI-779 on tumor progression in PyMT mice. Mice (n = 8) were subjected to 4 weeks of dosing with either vehicle or 5 and 25 mg/kg i.v. CCI-779, once weekly, starting at 8 weeks of age. The progression of tumors (three-dimensional volume in mm^3) was monitored by ultrasound. B, correlation of tumor volume (determined by ultrasound) and the total tumor burdens (by weight). After ultrasound assessment of the tumor volume at the end of the study, all of the identifiable tumors were dissected, and the weight was measured from a total of 27 animals collected from three individual studies. Each dot represents one animal, and the data are plotted to determine their correlation. *, $p < 0.05$; **, $p < 0.001$, compared with the vehicle-treated group.

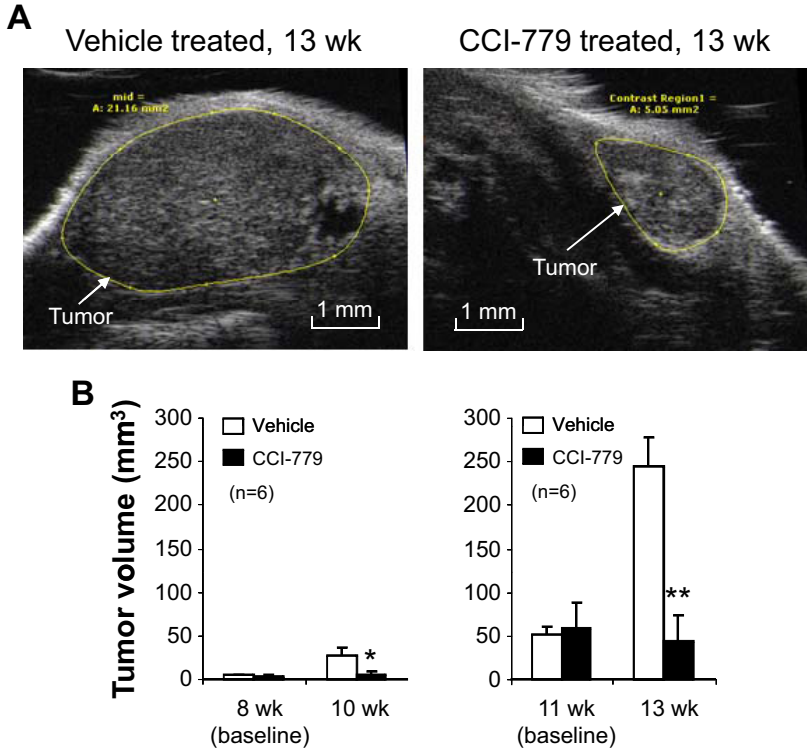

Fig. 5. Effects of CCI-779 on early and advanced tumors in PyMT mice by ultrasound analysis. PyMT mice at early (8–10 weeks) and advanced (11–13 weeks) stages of tumors were subjected to 2 weeks of treatment of either vehicle or 25 mg/kg i.v. CCI-779 once weekly. Tumor volumes on the single largest tumors were determined by ultrasound before dosing and at the end of the study. A, representative ultrasound images on vehicle- and CCI-779-treated animals are illustrated. Tumor area of ultrasound image was defined by the operator (as indicated by the arrow) and quantified by the software program provided by the vendor of the instrument as described in detail under *Materials and Methods*. B, tumor volume was acquired through three-dimensional reconstruction of two-dimensional tumor panels uniformly spaced at defined intervals using the software provided by the manufacturer. *, $p < 0.05$; **, $p < 0.001$, compared with the vehicle-treated group in the paired studies.

once each week) are illustrated in Fig. 7A. Significant reduction in macrophage burden was observed in tumors from mice treated with CCI-779, 46 ± 19% decrease at 13 weeks compared with vehicle treatment ($p < 0.05$; $n = 6$; Fig. 7B). A more moderate reduction in macrophage burden was observed in the early tumors (8–10 weeks; p not significant). There was a significant increase in macrophage burden along with the tumor progression (57.9% increase from 10 to 13 weeks; $p < 0.05$; $n = 7$–9), as reflected the change of macrophage staining from 2.4 ± 0.4 and 3.8 ± 0.5% for the early (10 weeks) and late (13 weeks) tumors, respectively, in the vehicle-treated mice. However, there were no changes in macrophage burden in the CCI-779-treated groups, with 1.9 ± 0.3 to 2.0 ± 0.4%, respectively, for the early and late stages of tumors (Fig. 7B).

Discussion

The studies presented in this article have been designed to address important aspects of preclinical drug transition into clinical development by seeking a more congruent animal model of breast cancer combined with biomarkers that allow more rigorous prediction of efficacy and confirmation of engagement of the compound with its signaling pathway elements by using

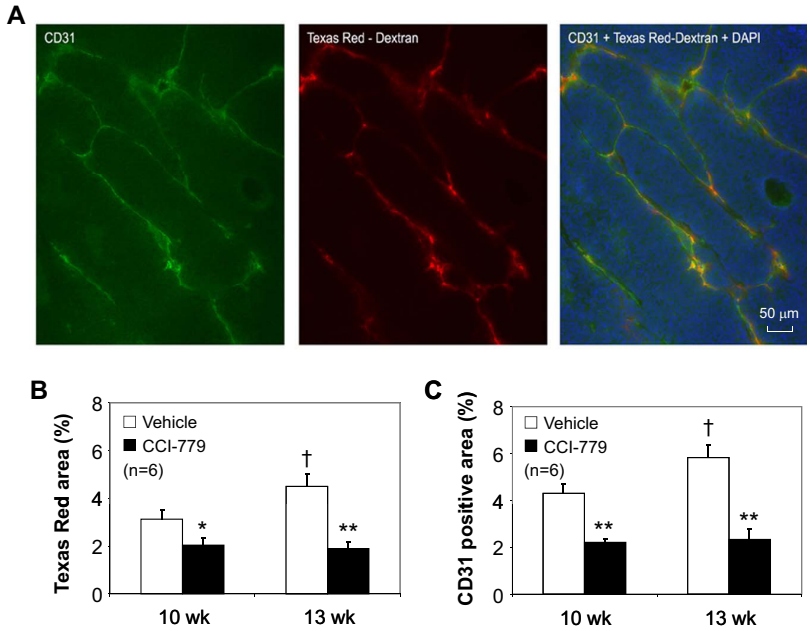

Fig. 6. Suppression of tumor vascular density after CCI-779 treatment in PyMT mice. A, illustration of representative images of immunohistochemical staining for CD31, Texas red-dextran, and their overlay with DAPI in tumors from 13-week-old mice. For best quality, frozen tissue sections were used for CD31 immunohistochemistry, and the immediately adjacent section was fixed in 10% formalin and processed for the fluorescent detection of vascular perfusion based on Texas red-dextran. B and C, quantitative data ($n = 6$) for Texas red-dextran (B) and CD31-positive (C) vascular areas. Images from entire tumors were captured, and at least three sections were used to generate the quantitative data. *, $p < 0.05$; **, $p < 0.001$, compared with the vehicle-treated group in the paired studies. †, $p < 0.05$, compared with vehicle-treated animals at 10 weeks of age.

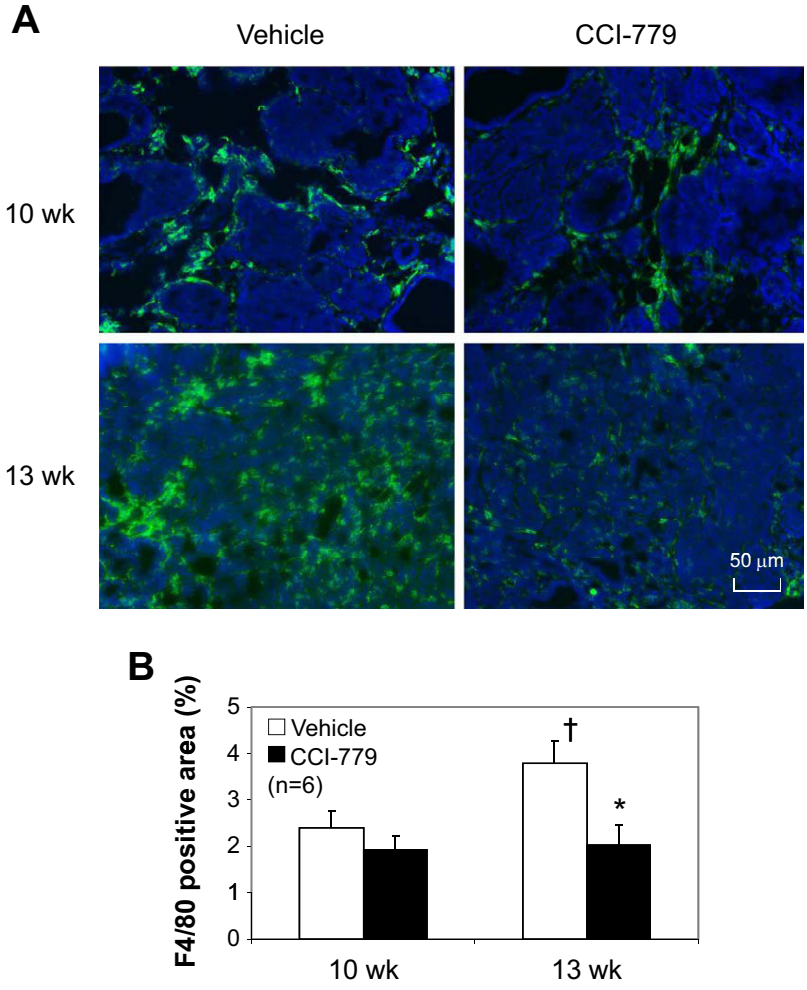

Fig. 7. Reduction of macrophage infiltration in tumors after CCI-779 treatment. Anti-F4/80 antibody was used to detect macrophages in the tumors of PyMT mice as described under *Materials and Methods*. A, representation immunohistochemical images after 2-week treatment of either vehicle or CCI-779 in 10- and 13-week-old mice. Green, macrophage (F4/80) signal; blue, DAPI counter staining for cell nuclei. B, quantitative data for the areas of macrophage immunostaining. Images from entire tumors ($n = 6$) were captured, and at least three sections were used to generate the quantitative data. *, $p < 0.05$, compared with the vehicle-treated group at the same age; †, $p < 0.05$, compared with vehicle-treated animals at 10 weeks of age.

multimodal biomarker imaging and pharmacological and biochemical approaches. Our data demonstrated for the first time that the potent and selective mTOR inhibitor CCI-779 is highly efficacious in arresting tumor progression in the PyMT mouse model of mammary carcinoma. The relative PK profiles of CCI-779 and rapamycin observed in the present study are in agreement with those observed in patients with breast and/or renal cancers (Raymond et al., 2004; Boni et al., 2005). The antitumor efficacy of CCI-779 was associated with significantly suppressed tumor vascular density and macrophage burden (Figs. 6 and 7), two key microenvironmental elements associated with tumor progression (Leek and Harris, 2002; Furuya and Yonemitsu, 2008; Li et al., 2008; De Palma and Lewis, 2011). Our present study not only confirmed a previous report for the antitumor activity of rapamycin in a transgenic mouse model of ErbB2-dependent human breast cancer (Liu et al., 2005), but also provided novel information on macrophage infiltration and PK/pharmacodynamic correlation of CCI-779.

The precise mechanisms of CCI-779 antitumor progression efficacy in PyMT mice remain to be elucidated. Our current knowledge of mTOR signaling pathway in tumorgenesis suggests several potential mechanisms of CCI-779 in blocking tumor progression. First, CCI-779 and rapamycin are known to be potent inhibitors of the mTOR complex 1, which is known to play a role in controlling cell autonomous growth, in response to diverse extracellular signals, including growth factors and nutrients (Chiang and Abraham, 2007; Le Tourneau et al., 2008; Guertin and Sabatini, 2009). The expression and activation state of several key components of the mTOR signaling pathway was demonstrated in the mammary tumors of PyMT mice (Fig. 1). Thus, one potential mechanism of CCI-779 in suppressing tumor growth in this PyMT model might be associated with its down-regulation of the PI3K/Akt/mTOR pathway. Data provided in this article demonstrated inhibition by CCI-779 of both phospho-S6 proteins in the tumors (Fig. 3), which is also in agreement with a previous report that demonstrated a direct role of CCI-779 in the repression of global protein synthesis (Shor et al., 2008).

Second, mTOR is also known to be downstream of the VEGF receptor signaling pathway, and mTOR inhibitors such as CCI-779 and rapamycin were shown to be antiangiogenic (Heng and Bukowski, 2008; Li et al., 2008). Rapamycin and related mTOR inhibitors inhibit endothelial cell VEGF expression and VEGF-induced endothelial cell proliferation (Dormond et al., 2007). CCI-779 has been reported to have antiangiogenic activity in a Matrigel assay in vivo (Del Bufalo et al., 2006) and also in a mouse xenograft model (Wan et al., 2006). In agreement with these previous findings, our present study provides more direct evidence that treatment of PyMT mice with CCI-779 significantly reduced tumor vascular density (Fig. 6). It also should be pointed out that the antiangiogenic effects of rapamycin may represent a downstream consequence of mTOR inhibition on

the tumor cells (production of proangiogenic cytokines) rather than on the tumor vasculature itself in a xenograft model (Amornphimoltham et al., 2008).

Third, the antitumor effects of CCI-779 in PyMT mice might have been, at least in part, associated with the reduction in tumor macrophage burden. In particular, macrophages infiltrated in tumors have been recently demonstrated to play a critical role in tumor chemoresistance (De Palma and Lewis, 2011). A previous study demonstrated that infiltrated macrophages in primary mammary tumors play a causal role in promoting tumor angiogenesis and the progression to malignancy in PyMT mice (Lin et al., 2006). In this regard, VEGF produced by macrophages has been suggested to play a key role in this process (Lin et al., 2007). In the present work, we have documented the increase in the number of macrophages in the primary mammary tumors along with tumor progression in PyMT mice (from early to late stages; Fig. 7). CCI-779 treatment markedly suppressed macrophage content, especially in the advanced tumors (from 11 to 13 weeks) (Fig. 7). In contrast to the late time point, the effect of CCI-779 on macrophage accumulation in tumors at 10 weeks was much less. The reason associated with this differential effect is not known. It might be involved in the different tumor microenvironment and/or the subpopulations of macrophages. Because CCI-779 suppressed tumor growth in both early and late stages, it is likely that macrophages in the early stage might be more resistant to CCI-779. At least two subtypes of macrophages (M1 and M2 types) have been characterized in tumors (Leek and Harris, 2002; Allavena et al., 2008). However, their potential differential distribution and response in the tumors to CCI-779 treatment remain to be investigated.

Taken together, this work illustrates the utility of biomarkers that report on the mechanism of action (mTOR in respect to survival pathway) and tumor environment growth-promoting elements (vasculogenesis and macrophage burden) in tandem with the tumor growth arrest efficacy of a compound in early and late tumor stages. The data from this PyMT model with immune competency may provide a better value for drug discovery and translational research of human disease.

Acknowledgments

We thank Salvatore Alesci, Daniel Johnston, Jay Gibbons, and Hans Peter Gerber (Pfizer Inc.) for helpful comments and discussions; and the staff at BioResources at the Pfizer Inc., Collegeville facility for excellent technical support with animal care and husbandry.

Authorship Contributions

Participated in research design: Wang, Zhan, Zhao, Alvarez, Zhou, Abraham, and Feuerstein.

Conducted experiments: Wang, Zhan, and Zhao.

Performed data analysis: Wang, Zhan, Zhao, and Chaudhary.

Wrote or contributed to the writing of the manuscript: Wang, Zhan, Zhao, Alvarez, Zhou, Abraham, and Feuerstein.

References

Abraham RT and Eng CH (2008) Mammalian target of rapamycin as a therapeutic target in oncology. *Expert Opin Ther Targets* **12:**209–222.

Allavena P, Sica A, Garlanda C, and Mantovani A (2008) The Yin-Yang of tumor-associated macrophages in neoplastic progression and immune surveillance. *Immunol Rev* **222:**155–161.

Amornphimoltham P, Patel V, Leelahavanichkul K, Abraham RT, and Gutkind JS (2008) A retroinhibition approach reveals a tumor cell-autonomous response to rapamycin in head and neck cancer. *Cancer Res* **68:**1144–1153.

Boni JP, Leister C, Bender G, Fitzpatrick V, Twine N, Stover J, Dorner A, Immermann F, and Burczynski ME (2005) Population pharmacokinetics of CCI-779: correlations to safety and pharmacogenomic responses in patients with advanced renal cancer. *Clin Pharmacol Ther* **77:**76–89.

Brown EJ, Beal PA, Keith CT, Chen J, Shin TB, and Schreiber SL (1995) Control of p70 s6 kinase by kinase activity of FRAP in vivo. *Nature* **377:**441–446.

Brown EJ and Schreiber SL (1996) A signaling pathway to translational control. *Cell* **86:**517–520.

Chiang GG and Abraham RT (2007) Targeting the mTOR signaling network in cancer. *Trends Mol Med* **13:**433–442.

Del Bufalo D, Ciuffreda L, Trisciuoglio D, Desideri M, Cognetti F, Zupi G, and Milella M (2006) Antiangiogenic potential of the mammalian target of rapamycin inhibitor temsirolimus. *Cancer Res* **66:**5549–5554.

De Palma M and Lewis CE (2011) Cancer: macrophages limit chemotherapy. *Nature* **472:**303–304.

Dormond O, Madsen JC, and Briscoe DM (2007) The effects of mTOR-Akt interactions on anti-apoptotic signaling in vascular endothelial cells. *J Biol Chem* **282:** 23679–23686.

Frost P, Moatamed F, Hoang B, Shi Y, Gera J, Yan H, Frost P, Gibbons J, and Lichtenstein A (2004) In vivo antitumor effects of the mTOR inhibitor CCI-779 against human multiple myeloma cells in a xenograft model. *Blood* **104:**4181–4187.

Fung AS, Wu L, and Tannock IF (2009) Concurrent and sequential administration of chemotherapy and the mammalian target of rapamycin inhibitor temsirolimus in human cancer cells and xenografts. *Clin Cancer Res* **15:**5389–5395.

Furuya M and Yonemitsu Y (2008) Cancer neovascularization and proinflammatory microenvironments. *Curr Cancer Drug Targets* **8:**253–265.

Geoerger B, Kerr K, Tang CB, Fung KM, Powell B, Sutton LN, Phillips PC, and Janss AJ (2001) Antitumor activity of the rapamycin analog CCI-779 in human primitive neuroectodermal tumor/medulloblastoma models as single agent and in combination chemotherapy. *Cancer Res* **61:**1527–1532.

Grote T, Siwak DR, Fritsche HA, Joy C, Mills GB, Simeone D, Whitcomb DC, and Logsdon CD (2008) Validation of reverse phase protein array for practical screening of potential biomarkers in serum and plasma: accurate detection of CA19–9 levels in pancreatic cancer. *Proteomics* **8:**3051–3060.

Guertin DA and Sabatini DM (2009) The pharmacology of mTOR inhibition. *Sci Signal* **2:**pe24.

Guy CT, Cardiff RD, and Muller WJ (1992) Induction of mammary tumors by expression of polyomavirus middle T oncogene: a transgenic mouse model for metastatic disease. *Mol Cell Biol* **12:**954–961.

Heng DY and Bukowski RM (2008) Anti-angiogenic targets in the treatment of advanced renal cell carcinoma. *Curr Cancer Drug Targets* **8:**676–682.

Huang S, Bjornsti MA, and Houghton PJ (2003) Rapamycins: mechanism of action and cellular resistance. *Cancer Biol Ther* **2:**222–232.

Institute of Laboratory Animal Resources (1996) *Guide for the Care and Use of Laboratory Animals* 7th ed. Institute of Laboratory Animal Resources, Commission on Life Sciences, National Research Council, Washington DC.

Le Tourneau C, Faivre S, Serova M, and Raymond E (2008) mTORC1 inhibitors: is temsirolimus in renal cancer telling us how they really work? *Br J Cancer* **99:** 1197–1203.

Leek RD and Harris AL (2002) Tumor-associated macrophages in breast cancer. *J Mammary Gland Biol Neoplasia* **7:**177–189.

Li WW, Hutnik M, and Gehr G (2008) Antiangiogenesis in haematological malignancies. *Br J Haematol* **143:**622–631.

Lin EY, Jones JG, Li P, Zhu L, Whitney KD, Muller WJ, and Pollard JW (2003) Progression to malignancy in the polyoma middle T oncoprotein mouse breast cancer model provides a reliable model for human diseases. *Am J Pathol* **163:** 2113–2126.

Lin EY, Li JF, Bricard G, Wang W, Deng Y, Sellers R, Porcelli SA, and Pollard JW (2007) Vascular endothelial growth factor restores delayed tumor progression in tumors depleted of macrophages. *Mol Oncol* **1:**288–302.

Lin EY, Li JF, Gnatovskiy L, Deng Y, Zhu L, Grzesik DA, Qian H, Xue XN, and Pollard JW (2006) Macrophages regulate the angiogenic switch in a mouse model of breast cancer. *Cancer Res* **66:**11238–11246.

Liu M, Howes A, Lesperance J, Stallcup WB, Hauser CA, Kadoya K, Oshima RG, and Abraham RT (2005) Antitumor activity of rapamycin in a transgenic mouse model of ErbB2-dependent human breast cancer. *Cancer Res* **65:**5325–5336.

Maglione JE, Moghanaki D, Young LJ, Manner CK, Ellies LG, Joseph SO, Nicholson B, Cardiff RD, and MacLeod CL (2001) Transgenic polyoma middle-T mice model premalignant mammary disease. *Cancer Res* **61:**8298–8305.

Neshat MS, Mellinghoff IK, Tran C, Stiles B, Thomas G, Petersen R, Frost P, Gibbons JJ, Wu H, and Sawyers CL (2001) Enhanced sensitivity of PTEN-deficient tumors to inhibition of FRAP/mTOR. *Proc Natl Acad Sci U S A* **98:**10314–10319.

Podsypanina K, Lee RT, Politis C, Hennessy I, Crane A, Puc J, Neshat M, Wang H, Yang L, Gibbons J, et al. (2001) An inhibitor of mTOR reduces neoplasia and normalizes p70/S6 kinase activity in Pten+/− mice. *Proc Natl Acad Sci U S A* **98:**10320–10325.

Raymond E, Alexandre J, Faivre S, Vera K, Materman E, Boni J, Leister C, Korth-Bradley J, Hanauske A, and Armand JP (2004) Safety and pharmacokinetics of escalated doses of weekly intravenous infusion of CCI-779, a novel mTOR inhibitor, in patients with cancer. *J Clin Oncol* **22:**2336–2347.

Sehgal SN, Molnar-Kimber K, Ocain TD, and Weichman BM (1994) Rapamycin: a novel immunosuppressive macrolide. *Med Res Rev* **14:**1–22.

Shor B, Zhang WG, Toral-Barza L, Lucas J, Abraham RT, Gibbons JJ, and Yu K (2008) A new pharmacologic action of CCI-779 involves FKBP12-independent inhibition of mTOR kinase activity and profound repression of global protein synthesis. *Cancer Res* **68:**2934–2943.

Teachey DT, Obzut DA, Cooperman J, Fang J, Carroll M, Choi JK, Houghton PJ, Brown VI, and Grupp SA (2006) The mTOR inhibitor CCI-779 induces apoptosis and inhibits growth in preclinical models of primary adult human ALL. *Blood* **107:**1149–1155.

Wan X, Shen N, Mendoza A, Khanna C, and Helman LJ (2006) CCI-779 inhibits rhabdomyosarcoma xenograft growth by an antiangiogenic mechanism linked to the targeting of mTOR/Hif-1α/VEGF signaling. *Neoplasia* **8:**394–401.

Wang X, Wang H, Xu L, Rozanski DJ, Sugawara T, Chan PH, Trzaskos JM, and Feuerstein GZ (2003) Significant neuroprotection against ischemic brain injury by inhibition of the MEK1 protein kinase in mice: exploration of potential mechanism associated with apoptosis. *J Pharmacol Exp Ther* **304:**172–178.

Yu K, Toral-Barza L, Discafani C, Zhang WG, Skotnicki J, Frost P, and Gibbons JJ (2001) mTOR, a novel target in breast cancer: the effect of CCI-779, an mTOR inhibitor, in preclinical models of breast cancer. *Endocr Relat Cancer* **8:**249–258.

Zhao L, Zhan Y, Rutkowski JL, Feuerstein GZ, and Wang X (2010) Correlation between 2- and 3-dimensional assessment of tumor volume and vascular density by ultrasonography in a transgenic mouse model of mammary carcinoma. *J Ultrasound Med* **29:**587–595.

Address correspondence to: Dr. Xinkang Wang, Translational Science, Agennix Incorporated, 101 College Road East, Princeton, NJ 08540. E-mail: wangxk2000@yahoo.com